

## Central BH mass of tidal disruption event candidate SDSS J0159 through long-term optical variabilities

XUEGUANG ZHANG<sup>\*1</sup>

<sup>1</sup>Guangxi Key Laboratory for Relativistic Astrophysics, School of Physical Science and Technology, GuangXi University, No. 100, Daxue Road, Nanning, 530004, P. R. China

Submitted to ApJ

### ABSTRACT

In this manuscript, central BH mass is determined in the tidal disruption event (TDE) candidate SDSS J0159, through the nine years long variabilities, in order to check whether the virial BH mass is consistent with the mass estimated by another independent methods. First, host galaxy spectroscopic features are described by 350 simple stellar templates, to confirm the total stellar mass about  $7 \times 10^{10} M_{\odot}$  in SDSS J0159, indicating the virial BH mass about two magnitudes larger than the BH mass estimated by the total stellar mass. Second, based on an efficient method and fitting procedure, through theoretical TDE model applied to describe the SDSS *ugriz*-band light curves of SDSS J0159, central BH mass can be determined as  $M_{BH} \sim 4.5^{+1.3}_{-1.1} \times 10^6 M_{\odot}$ , well consistent with the M-sigma relation expected BH mass and the total stellar mass expected BH mass. Third, the theoretical TDE model with parameter of central BH mass limited to be higher than  $10^8 M_{\odot}$  can not lead to reasonable descriptions to the light curves of SDSS J0159, indicating central BH mass higher than  $10^8 M_{\odot}$  is not preferred in SDSS J0159. Therefore, the TDE model determined central BH mass of SDSS J0159 are about two magnitudes lower than the virial BH mass, to support central BLRs including accreting debris contributions from central TDE, and provide interesting clues to reconfirm that outliers in the space of virial BH mass versus stellar velocity dispersion should be better candidates of TDE.

*Keywords:* active galactic nuclei – emission line galaxies – supermassive black holes – tidal disruption – transient sources

### 1. INTRODUCTION

SDSS J0159 (=SDSS J015957.64+003310.5) at redshift  $z = 0.312$  (corresponding luminosity distance about 1625Mpc) is an interesting object in the literature. LaMassa et al. (2015) have reported the SDSS J0159 as the first changing-look quasar transitioned from a Type 1 quasar (both apparent broad H $\alpha$  and H $\beta$  in optical spectrum) to a Type 1.9 AGN (Active Galactic Nuclei) (only weak broad H $\alpha$  in optical spectrum) between 2000 and 2010, and reported the dimming of the AGN continuum as intrinsic physical reason to explain the changing-look properties. Meanwhile, Merloni et al. (2015) have reported the SDSS J0159 as a candidate of Tidal Disruption Event (TDE) due to the very rapid rise and the decay trend of the long-term optical variabilities well described by  $t^{-5/3}$  expected by theoretical TDE model, indicating TDEs can be well treated as one explanation to

changing-look AGN as discussed in Yang et al. (2018); Zhang (2021b).

A star can be tidally disrupted by gravitational tidal force of a central massive black hole (BH), when it passing close to the central BH with a distance larger than event horizon of the BH but smaller than the expected tidal disruption radius  $R_T = R_{\star} \times (\frac{M_{BH}}{M_{\star}})^{1/3}$ , where  $R_{\star}$ ,  $M_{\star}$  and  $M_{BH}$  represent radius and mass of the tidally disrupted star and central BH mass, respectively. And then, fallback materials from tidally disrupted star can be accreted by the central massive BH, leading to a flare up follows by a decrease. This is the basic picture of a TDE.

The well-known pioneer work on TDE can be found in Rees (1988). Since then, as an excellent beacon for indicating massive black holes, both theoretical simulations and observational results on TDEs have been widely studied and reported in the literature. More detailed and improved simulations on TDEs can be found in Evans & Kochanek (1989); Magorrian & Tremaine (1999); Bogdanovic et al. (2004); Lodato et al. (2009);

MacLeod et al. (2012); Guillochon & Ramirez-Ruiz (2015); Lodato et al. (2015); Bonnerot et al. (2017); Darbha et al. (2018); Coughlin & Nixon (2019); Curd & Narayan (2019); Golightly et al. (2019), etc.. More recent reviews in detail on TDEs can be found in Stone et al. (2018). And based on theoretical TDE model, public codes of *TDEFIT* provided by Guillochon et al. (2014) (<https://github.com/guillochontdefit>) and *MOSFIT* provided by Guillochon et al. (2018) (<https://github.com/guillochon/mosfit>) have been well applied to describe both structure evolutions in details for the falling back stellar debris and evolutions of expected time-dependent long-term variability through hydrodynamical simulations. Therefore, TDE models with sufficient model parameters can be applied to describe observed long-term variability from TDEs.

Meanwhile, there are so-far around one hundred observational results on TDE candidates reported in the literature based on TDE expected variability properties in different multi-wavelength bands, such as the reported TDE candidates in Komossa et al. (2004); Cenko et al. (2012); Gezari et al. (2012); Holoien et al. (2014, 2016); Lin et al. (2017); Tadhunter et al. (2017); Mattila et al. (2018); Wang et al. (2018); Holoien et al. (2020); Liu et al. (2020); Neustadt et al. (2020); Goodwin et al. (2022), etc.. More recently, van Velzen et al. (2021) have reported seventeen TDE candidates from the First Half of ZTF (Zwicky Transient Facility) Survey observations along with Swift UV and X-ray follow-up observations. Sazonov et al. (2021) have reported thirteen TDE candidates from the SRG all-sky survey observations and then confirmed by follow-up optical observations. More recent review on observational properties of reported TDEs can be found in Gezari (2021).

Among the reported TDE candidates, SDSS J0159 is an interesting object, because its central virial BH mass reported as  $\sim 10^8 M_\odot$  in LaMassa et al. (2015); Merloni et al. (2015) through the virialization assumptions (Peterson et al. 2004; Greene & Ho 2005; Vestergaard & Peterson 2006; Kelly & Bechtold 2007; Rafiee & Hall 2011; Shen et al. 2011; Mejia-Restrepo et al. 2022) applied to BLRs (broad emission line regions) clouds, the largest BH mass among the reported BH masses of TDE candidates in Wevers et al. (2017); Mockler et al. (2019); Zhou et al. (2021); Wong et al. (2022). However, variations of accretion flows have apparent effects on dynamical structures of BLRs, if the BLRs clouds are tightly related to TDEs, such as the more detailed abnormal variabilities of broad emission lines in the TDE candidate ASASSN-14li in Holoien et al. (2016): strong emissions leading to wider line widths of broad  $H\alpha$  which are against the expected results by the Virialization assumptions to BLRs clouds. More recently, Zhang et al. (2019) have measured the stellar velocity dispersion about  $81 \pm 27 \text{ km/s}$  of

SDSS J0159 through the absorption features around  $4000\text{\AA}$ , reported that the M-sigma relation (Ferrarese & Merritt 2000; Gebhardt et al. 2000; Kormendy & Ho 2013; Bennert et al. 2015) determined central BH mass are about two magnitudes smaller than the virial BH mass in SDSS J0159, and provided an interesting clue to detect TDE candidates by outliers in the space of virial BH masses versus stellar velocity dispersions.

Moreover, Charlton et al. (2019) have shown the total stellar mass of SDSS J0159 is about  $4.7 \times 10^{10} M_\odot$ , indicating the central BH mass about  $6 \times 10^6 M_\odot$  (the accepted value in Wong et al. (2022)) in SDSS J0159 through the correlation between central BH mass and total stellar mass as discussed in Haring & Rix (2004); Sani et al. (2011); Kormendy & Ho (2013); Reines & Volonteri (2015), roughly consistent with the BH mass estimated by the M-sigma relation reported in our previous paper Zhang et al. (2019). Therefore, besides the virial BH mass through virialization assumption to BLRs clouds and the BH mass through the M-sigma relation and through the total stellar mass, BH mass of SDSS J0159 determined through one another independent method will be very interesting and meaningful.

More recently, Guillochon et al. (2014); Mockler et al. (2019); Ryu et al. (2020); Zhou et al. (2021) have shown that the long-term TDE model expected time-dependent variability properties can be well applied to estimate central BH masses of TDE candidates. However, SDSS J0159 is not discussed in Mockler et al. (2019); Ryu et al. (2020); Zhou et al. (2021), probably due to lack of information of peak intensities of light curves in SDSS J0159 and/or other unknown reasons. Therefore, in the manuscript, the central BH mass of SDSS J0159 is to be estimated by theoretical TDE model applied to describe the long-term optical variabilities. It is very interesting to check whether would the reported virial BH mass or M-sigma relation determined BH mass be coincident with the TDE model determined BH mass. The manuscript is organized as follows. In section 2, we present spectroscopic features of SDSS J0159, in order to re-confirm the low stellar velocity dispersion and the low total stellar mass. Section 3 shows our methods with a TDE model applied to describe observed multi-band light curves. Then, the main results and necessary discussions are shown in Section 4. Section 5 shows simulating results to check whether the long-term variabilities are tightly related to a central TDE in SDSS J0159. Section 6 gives our main summary and final conclusions. And in the manuscript, the cosmological parameters of  $H_0 = 70 \text{ km} \cdot \text{s}^{-1} \text{ Mpc}^{-1}$ ,  $\Omega_\Lambda = 0.7$  and  $\Omega_m = 0.3$  have been adopted.

## 2. SPECTROSCOPIC RESULTS OF SDSS J0159

In Zhang et al. (2019), the stellar velocity dispersion about  $81 \pm 27 \text{ km/s}$  of SDSS J0159 has been measured through absorption features around  $4000\text{\AA}$  in the

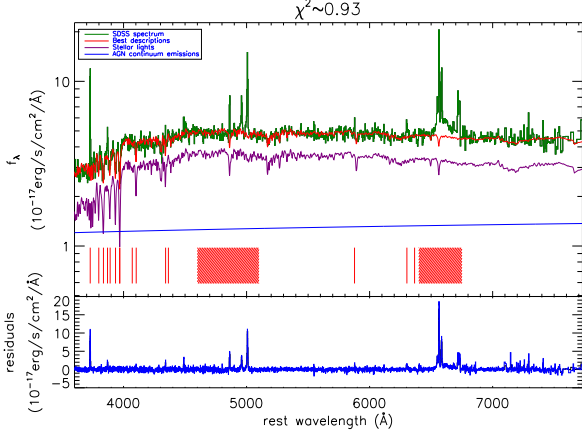


**Figure 1.** The SDSS spectrum (solid dark green line) of SDSS J0159 and the best descriptions (solid red line) to the spectrum with the emission lines being masked out by the SSP method with applications of 350 stellar templates. In top region, as shown legend in top-left corner, solid purple line shows the SSP method determined stellar lights, and solid blue line shows the determined power law AGN continuum emissions, vertical red lines from left to right mark the following emission features masked out, including [O II] $\lambda$ 3727Å, H $\theta$ , H $\eta$ , [Ne III] $\lambda$ 3869Å, He I $\lambda$ 3891Å, Calcium K line, [Ne III] $\lambda$ 3968Å, Calcium H line, [S II] $\lambda$ 4070Å, H $\delta$ , H $\gamma$ , [O III] $\lambda$ 4364Å, He I $\lambda$ 5877Å and [O I] $\lambda$ 6300, 6363Å, respectively, and the area filled by red lines around 5000Å shows the region masked out including the emission features of probable He II, broad and narrow H $\beta$  and [O III] doublet, and the area filled by red lines around 6550Å shows the region masked out including the emission features of broad and narrow H $\alpha$ , [N II] and [S II] doublets. Bottom region shows the residuals calculated by SDSS spectrum minus sum of the stellar lights and the power law continuum emissions.

SDSS spectrum with plate-mjd-fiberid=3609-55201-0524 which includes apparent host galaxy contributions, based on the 39 simple stellar population templates from the Bruzual & Charlot (2003). In the section, the SSP (simple Stellar Population) method discussed in Bruzual & Charlot (1993); Kauffmann et al. (2003b); Cappellari & Emsellem (2004); Cid Fernandes et al. (2005, 2013); Zhang (2014); Lopez Fernandez et al. (2016); Cappellari (2017); Werle (2019) is re-applied to mainly determine the total stellar mass in SDSS J0159 but with more plenty of stellar templates, in order to check whether are there low total stellar mass in SDSS J0159, which will provide further clues on central BH mass. In the section, the spectrum with plate-mjd-fiberid=3609-55201-0524 is mainly considered and collected from the eBOSS (Extended Baryon Oscillation Spectroscopic Survey) (Ahumada et al. 2020; Abdurro’uf et al. 2022), due to the following main reason. The eBOSS spectrum with apparent stellar absorption features of SDSS J0159 in the Type 1.9 AGN state is observed at the late times of the TDE expected flare, with few effects of TDE on the spectroscopic features.

Due to the weak but apparent broad H $\alpha$  in SDSS J0159 observed in mjd=55201, contributions from central AGN continuum emissions should be considered. Here, 350 SSP templates  $S_{lib}$  are collected from the MILES (Medium resolution INT Library of Empirical Spectra) stellar library (Falcon-Barroso et al. 2011; Knowles et al. 2021) with 50 stellar ages from 0.06Gyrs to 17.78Gyrs and with 7 metallicities from -2.32 to 0.22, and the simple SSP method is re-applied to determine the host galaxy stellar lights and the central AGN continuum emissions, through the following model function

$$S_g = A \otimes S_{lib,\sigma,V_s} + \alpha \times \lambda^\beta \quad (1)$$

with  $S_g$  as the SDSS spectrum of SDSS J0159,  $S_{lib,\sigma,V_s}$  as the broadened and shifted stellar templates with broadening velocity  $\sigma$  and shifting velocity  $V_s$ ,  $\alpha \times \lambda^\beta$  as the AGN continuum emissions. Then, through the Levenberg-Marquardt least-squares minimization technique (the known MPFIT package), with emission lines being masked out, the weights  $A$  and the power law continuum emissions can be well determined. Fig. 1 shows the best descriptions and corresponding residuals to the SDSS spectrum with rest wavelength range from 3650Å to 7700Å by the model function above, with  $\chi^2 \sim 0.93$  (summed squared residuals divided by degree of freedom) and with residuals calculated by SDSS spectrum minus the best descriptions.

Based on the best descriptions, total stellar mass is determined to be about

$$M_{tot} \sim \sum A \times 4\pi Dis^2./Unit/L_\odot \sim 7.11 \times 10^{10} M_\odot \quad (2)$$

with  $L_\odot = 3.826 \times 10^{33}$  erg/s as the solar luminosity, and  $Dis = 1623 Mpc$  as the distance between SDSS J0159 and the earth, and  $Unit = 10^{-17}$  erg/s/cm $^2$ /Å as the emission intensity unit of the SDSS spectrum. The calculated total stellar mass in SDSS J0159 is roughly consistent with the reported  $4.7^{+8.0}_{-3.9} \times 10^{10} M_\odot$  in Charlton et al. (2019) and the reported  $2.3^{+0.7}_{-0.1} \times 10^{10} M_\odot$  in Graur et al. (2018), indicating lower central BH mass in SDSS J0159.

Therefore, the low total stellar mass in SDSS J0159 can be well confirmed, and lead to expected lower central BH mass than the Virial BH mass in SDSS J0159. Then, besides the lower total stellar mass in SDSS J0159, it is interesting to check whether the TDE model can still lead to different central BH mass in SDSS J0159.

### 3. MAIN METHOD AND FITTING PROCEDURE TO DESCRIBE THE LIGHT CURVES

Similar as what we have recently done in Zhang (2022a) to describe X-ray variabilities in the TDE candidate *Swift* J2058.4+0516 with relativistic jet, the following four steps are applied to describe the long-term optical *ugriz*-band variabilities of SDSS J0159. The similar procedures have also

been applied in Zhang (2022b) to discuss TDE expected long-term variabilities in the high redshift quasar SDSS J014124+010306 and in Zhang (2022c) to discuss TDE expected long-term variabilities of broad H $\alpha$  line luminosity in the known changing-look AGN NGC 1097.

First, standard templates of viscous-delayed accretion rates in TDEs are created. Based on the discussed  $dM/dE$  provided in (Guillochon et al. 2014, 2018; Mockler et al. 2019) (the fundamental elements in the public code of TDEFIT and MOSFIT), templates of fallback material rate  $\dot{M}_{fbt} = dM/dE \times dE/dt$  can be calculated with  $dE/dt \sim \frac{(2\pi G M_{BH})^{2/3}}{3 t^{5/3}}$ , for the standard cases with central BH mass  $M_{BH} = 10^6 M_\odot$  and disrupted main-sequence star of  $M_* = 1 M_\odot$  and with a grid of the listed impact parameters  $\beta_t$  in Guillochon & Ramirez-Ruiz (2013). Considering the viscous delay effects as discussed in Guillochon & Ramirez-Ruiz (2013); Mockler et al. (2019) by the viscous timescale  $T_{vis}$ , templates of viscous-delayed accretion rates  $\dot{M}_{at}$  can be determined by

$$\dot{M}_{at} = \frac{\exp(-t/T_{vis})}{T_{vis}} \int_0^t \exp(t'/T_{vis}) \dot{M}_{fbt} dt' \quad (3)$$

. Here, a grid of 31  $\log(T_{vis}, t/\text{years})$  range from -3 to 0 are applied to create templates  $\dot{M}_{at}$  for each impact parameter. The final templates of  $\dot{M}_{at}$  include 736 (640) time-dependent viscous-delayed accretion rates for 31 different  $T_{vis}$  of each 23 (20) impact parameters for the main-sequence star with polytropic index  $\gamma$  of 4/3 (5/3).

Second, for common TDE cases with model parameters of  $\beta$  and  $T_{vis}$  different from the list values in  $\beta_t$  and in  $T_{vis}, t$ , the actual viscous-delayed accretion rates  $\dot{M}_a$  are created by the following two linear interpolations. Assuming that  $\beta_1, \beta_2$  in the  $\beta_t$  are the two values nearer to the input  $\beta$ , and that  $T_{vis1}, T_{vis2}$  in the  $T_{vis}, t$  are the two values nearer to the input  $T_{vis}$ , the first linear interpolation is applied to find the viscous-delayed accretion rates with input  $T_{vis}$  but with  $\beta = \beta_1$  and  $\beta = \beta_2$  by

$$\begin{aligned} \dot{M}_a(T_{vis}, \beta_1) &= \dot{M}_{at}(T_{vis1}, \beta_1) + \\ &\frac{T_{vis} - T_{vis1}}{T_{vis2} - T_{vis1}} (\dot{M}_{at}(T_{vis2}, \beta_1) - \dot{M}_{at}(T_{vis1}, \beta_1)) \\ \dot{M}_a(T_{vis}, \beta_2) &= \dot{M}_{at}(T_{vis1}, \beta_2) + \\ &\frac{T_{vis} - T_{vis1}}{T_{vis2} - T_{vis1}} (\dot{M}_{at}(T_{vis2}, \beta_2) - \dot{M}_{at}(T_{vis1}, \beta_2)) \end{aligned} \quad (4)$$

. Then, the second linear interpolation is applied to find the viscous-delayed accretion rates with input  $T_{vis}$  and with input  $\beta$  by

$$\begin{aligned} \dot{M}_a(T_{vis}, \beta) &= \dot{M}_a(T_{vis}, \beta_1) + \\ &\frac{\beta - \beta_1}{\beta_2 - \beta_1} (\dot{M}_a(T_{vis}, \beta_2) - \dot{M}_a(T_{vis}, \beta_1)) \end{aligned} \quad (5)$$

. Applications of the linear interpolations can save about one tenth of the running time for the fitting procedure to describe the observed long-term light curves, comparing with the running time for the fitting procedure considering the integral equation (3) to determine the  $\dot{M}_a(T_{vis}, \beta)$ .

Third, for a common TDE case with  $M_{BH}$  and  $M_*$  different from  $10^6 M_\odot$  and  $1 M_\odot$ , the actual viscous-delayed accretion rates  $\dot{M}$  and the corresponding time information in observer frame are created by the following scaling relations as shown in Guillochon et al. (2014); Mockler et al. (2019),

$$\begin{aligned} \dot{M} &= M_{BH,6}^{-0.5} \times M_*^2 \times R_*^{-1.5} \times \dot{M}_a(T_{vis}, \beta) \\ t_m &= (1+z) \times M_{BH,6}^{0.5} \times M_*^{-1} \times R_*^{1.5} \times t_a(T_{vis}, \beta) \end{aligned} \quad (6)$$

, where  $M_{BH,6}$ ,  $M_*$ ,  $R_*$  and  $z$  represent central BH mass in unit of  $10^6 M_\odot$ , stellar mass and radius in unit of  $M_\odot$  and  $R_\odot$ , and redshift of host galaxy of a TDE, respectively. And the mass-radius relation well discussed in Tout et al. (1996) is accepted for main-sequence stars.

Fourth, based on the calculated time-dependent templates of accretion rate  $\dot{M}(t)$ , the time dependent emission spectrum  $f_\lambda(t)$  can be calculated through the modeled simple black-body photosphere model discussed in Guillochon & Ramirez-Ruiz (2013); Mockler et al. (2019)

$$\begin{aligned} f_\lambda(t) &= \frac{2\pi G c^2}{\lambda^5} \frac{1}{\exp(\frac{hc}{k\lambda T_p(t)}) - 1} \left(\frac{R_p(t)}{Dis}\right)^2 \\ T_p(t) &= \left(\frac{\eta \dot{M}(t) c^2}{4\pi\sigma_{SB} R_p^2(t)}\right)^{1/4} \\ R_p(t) &= R_0 a_p \left(\frac{\eta \dot{M}(t) c^2}{1.3 \times 10^{38} M_{BH}}\right)^{l_p} \\ a_p &= (GM_{BH} \times \frac{t_p}{\pi})^{1/3} \end{aligned} \quad (7)$$

with  $Dis$  as the distance to the earth calculated by redshift,  $k$  as the Boltzmann constant,  $T_p(t)$  and  $R_p(t)$  as the time-dependent effective temperature and radius of the photosphere, respectively,  $\eta$  as the energy transfer efficiency smaller than 0.4,  $\sigma_{SB}$  as the Stefan-Boltzmann constant,  $t_p$  as the time information of the peak accretion rate. Then, based on the calculated time dependent  $f_\lambda(t)$  in observer frame and the wavelength ranges  $\lambda_{u, g, r, i, z}$  of SDSS *ugriz* filters, the SDSS *ugriz*-band time dependent luminosities as discussed in Merloni et al. (2015) can be calculated by

$$L_{u, g, r, i, z}(t) = \int_{\lambda_{u, g, r, i, z}} f_\lambda(t) d\lambda \times 4\pi \times Dis^2 \quad (8)$$

with  $Dis$  as the distance to the earth calculated by redshift. Here, not magnitudes but luminosities are calculated, mainly because that the collected light curves of SDSS J0159 are the time dependent *ugriz*-band luminosities.

Finally, the theoretical TDE model expected time dependent optical light curves  $L_{(u, g, r, i, z)}(t)$  can be described

by the following seven model parameters, the central BH mass  $\log(M_{\text{BH}}/10^6 M_{\odot})$ , the stellar mass  $\log(M_{\star})$  (corresponding stellar radius  $R_{\star}$  calculated by the mass-radius relation), the energy transfer efficiency  $\log(\eta)$ , the impact parameter  $\log(\beta)$ , the viscous timescale  $\log(T_{\text{vis}})$ , the parameters  $l_p$  and  $R_0$  related to the black-body photosphere model. Meanwhile, the redshift 0.312 of SDSS J0159 is accepted. Then, through the through the well-known maximum likelihood method combining with the Markov Chain Monte Carlo (MCMC) technique (Foreman-Mackey et al. 2013), the *ugriz*-band light curves of SDSS J0159 can be well described, with accepted prior uniform distributions and starting values of the model parameters listed in Table 1. Meanwhile, the available BH masses and stellar masses are the ones leading the determined tidal disruption radius  $R_{\text{TDE}}$ ,

$$\frac{R_{\text{TDE}}}{R_s} = 5.06 \times (M_{\star})^{-1/3} \left(\frac{M_{\text{BH},6}}{10}\right)^{-2/3} \times R_{\star} > 1 \quad (9)$$

, to be larger than event horizon of central BH ( $R_s = 2GM_{\text{BH}}/c^2$ ).

#### 4. MAIN RESULTS AND NECESSARY DISCUSSIONS

The observed light curves (the time dependent luminosities) in SDSS *ugriz* bands for SDSS J0159 are shown in Fig. 2 with the data points are directly collected from Table 2 in Merloni et al. (2015) after subtractions of host galaxy contributions. This is the main reason why the time dependent luminosities rather than the apparent magnitudes are collected, because the host galaxy contributions have been clearly removed from the time dependent luminosities. Then, based on the discussed method and fitting procedure in section above, the observed *ugriz*-band light curves of SDSS J0159 are simultaneously described by the theoretical TDE model with seven model parameters. Fig. 2 shows the best fitting results and the corresponding confidence bands after considerations of the uncertainties of model parameters based on the theoretical TDE model.

It is clear that besides the *z*-band light curve statistically lower than the theoretical TDE model expected values, the other *ugri*-bands light curves can be well described by the theoretical TDE model. However, as simply discussed in Guillochon & Ramirez-Ruiz (2013); Mockler et al. (2019), the simple black-body photosphere model can be well applied to describe optical band variabilities, considering the probable additional contributions of NIR emissions from dust clouds, the simple black-body black-body photosphere model is not preferred to describe the *z*-band variabilities. Certainly, a simply strengthened TDE model expected theoretical *z*-band light curve by a factor 2 (dot-dashed lines in the last panel of Fig. 2) can be well applied to describe the observed *z*-band light curve. Furthermore, as well discussed in Lu et al. (2016); Jiang et al. (2017, 2021), there

should be apparent IR contributions to *z*-band light curve of SDSS J0159 at  $z = 0.312$ , considering that radiation photons from the central TDE are absorbed by dust grains and then re-radiated in the infrared band, similar as discussed in Guillochon & Ramirez-Ruiz (2013); Mockler et al. (2019). In other words, if the additional contributions were removed, the *z*-band light curve obey the same TDE expected variability properties as those in *ugri*-bands.

Fig. 3 shows the MCMC technique determined two dimensional posterior distributions in contours of the seven model parameters. The accepted values of the model parameters are listed in Table 1. The central BH masses  $M_{\text{BH}} (10^6 M_{\odot})$  in SDSS J0159 are about  $\sim 5.7^{+0.8}_{-0.7}$  and  $\sim 3.3^{+0.5}_{-0.4}$  by applications of TDE model with  $\gamma = 4/3$  and with  $\gamma = 5/3$ , respectively. Moreover, comparing with the reported parameters for the TDE candidates in Mockler et al. (2019), the reported values of the model parameters are common values among the TDE candidates.

Before proceeding further, it is necessary to consider whether central BH with mass around  $10^8 M_{\odot}$  (the virial BH mass) can also lead to accepted descriptions to the *ugri*-band light curves<sup>1</sup> of SDSS J0159. Therefore, besides the best fitting results determined through the seven model parameters as free parameters with prior uniform distributions, the TDE model and the fitting procedure is running again, but with the central BH mass having the prior uniform distribution limited from  $1 \times 10^8 M_{\odot}$  to  $5 \times 10^8 M_{\odot}$  and the other model parameters having the same prior uniform distributions as what have been applied above. Then, the TDE model determined descriptions are shown as dotted purple lines and dotted pink lines in the first four panels of Fig. 2, which are worse to explain the rise-to-peak trend. However, if the first data point shown in Fig. 2 (MJD-50200=880) was not related to the expected central TDE (i.e., starting time of the expected central TDE was later than MJD-50200=880), the determined descriptions with accepted virial BH mass could be also well accepted. However, after considering the following two points, the data point at MJD-50200=880 is considered to be related to central transient event. First, as listed values in Table 2 in Merloni et al. (2015), the luminosity at MJD-50200=880 is at least about 2 times stronger than the data points at late times of the event with MJD-50200 later than 4000, indicating that the first data point at MJD-50200=880 related to central event is preferred in SDSS J0159. Second, the CSS (Drake et al. 2009) V-band photometric light curve at quiescent state of SDSS J0159 is collected and shown in bottom right panel of Fig 2. The CSS V-band light curve has standard deviation about 0.12mag, leading corresponding luminosity variability to be about 11.2%, quite smaller than the luminosity ratio

<sup>1</sup> Considering probable contributions from dust emissions, the *z*-band light curve is not considered here.

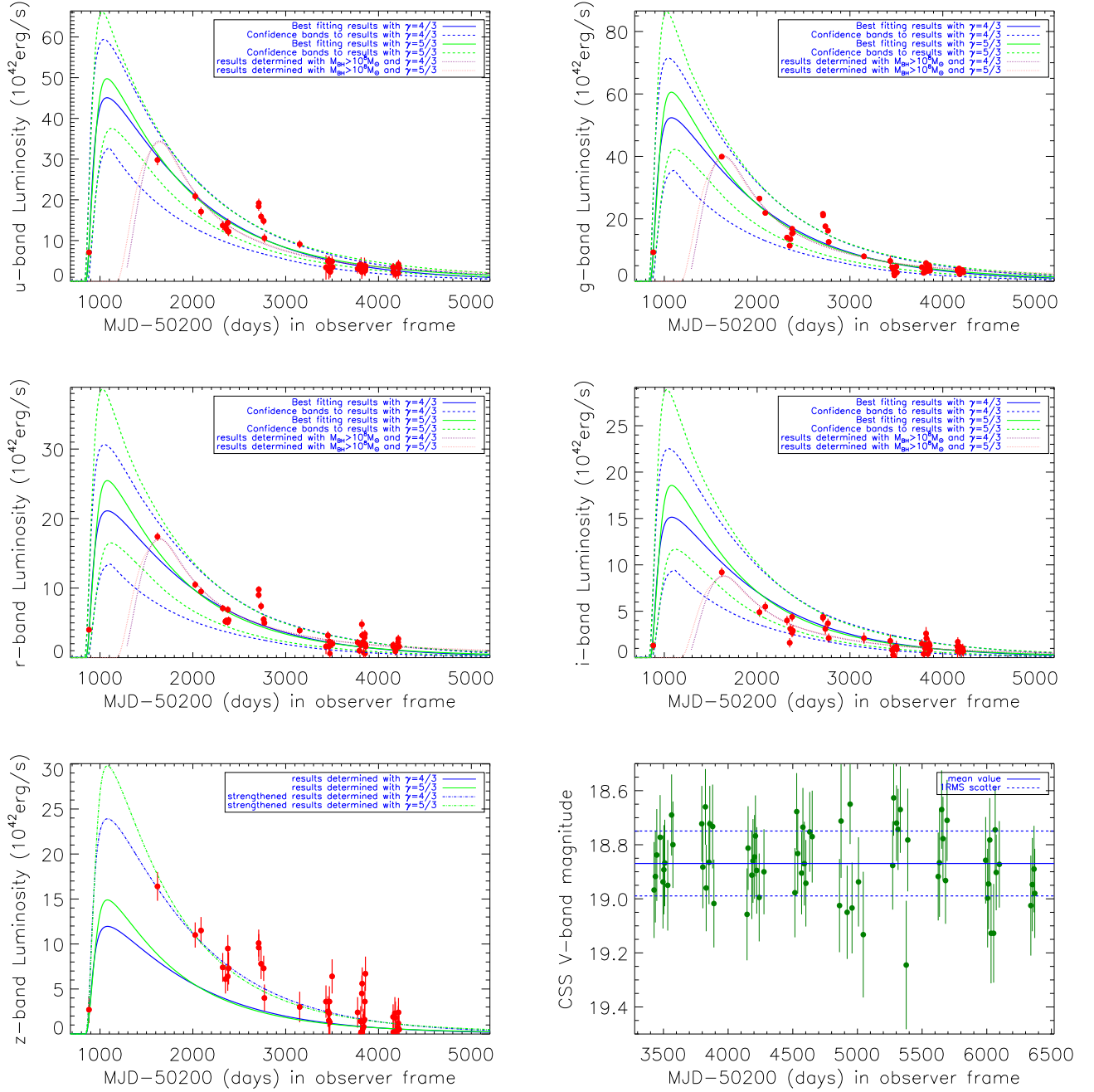


**Figure 2.** The first five panels show theoretical TDE model determined the best fitting results to the SDSS *ugriz*-band light curves (solid circles plus error bars in red) of SDSS J0159. In the panels for the *ugri*-band light curves, as shown legend in top right corner, solid blue line and dashed blue lines show the best fitting results and the corresponding confidence bands calculated by uncertainties of the model parameters determined by applications of TDE model with  $\gamma = 4/3$ , solid green line and dashed green lines show the best fitting results and the corresponding confidence bands determined by applications of TDE model with  $\gamma = 5/3$ , dotted line in purple and dotted line in pink show the TDE model determined descriptions to the light curve by applications of prior distribution of central BH mass larger than  $10^8 M_{\odot}$  in the TDE model with  $\gamma = 4/3$  and  $\gamma = 5/3$ , respectively. In the bottom left panel for the *z*-band light curve, as shown legend in top right corner, solid blue line and solid green line show the results determined by applications of TDE model with  $\gamma = 4/3$  and with  $\gamma = 5/3$ , respectively, dot-dashed blue line and dot-dashed green line show the corresponding strengthened model results by the factor of 2, which can be applied to well describe the *z*-band light curve. Bottom right panel shows the CSS V-band light curve, with horizontal solid and dashed lines show the mean value and corresponding 1RMS scatter.

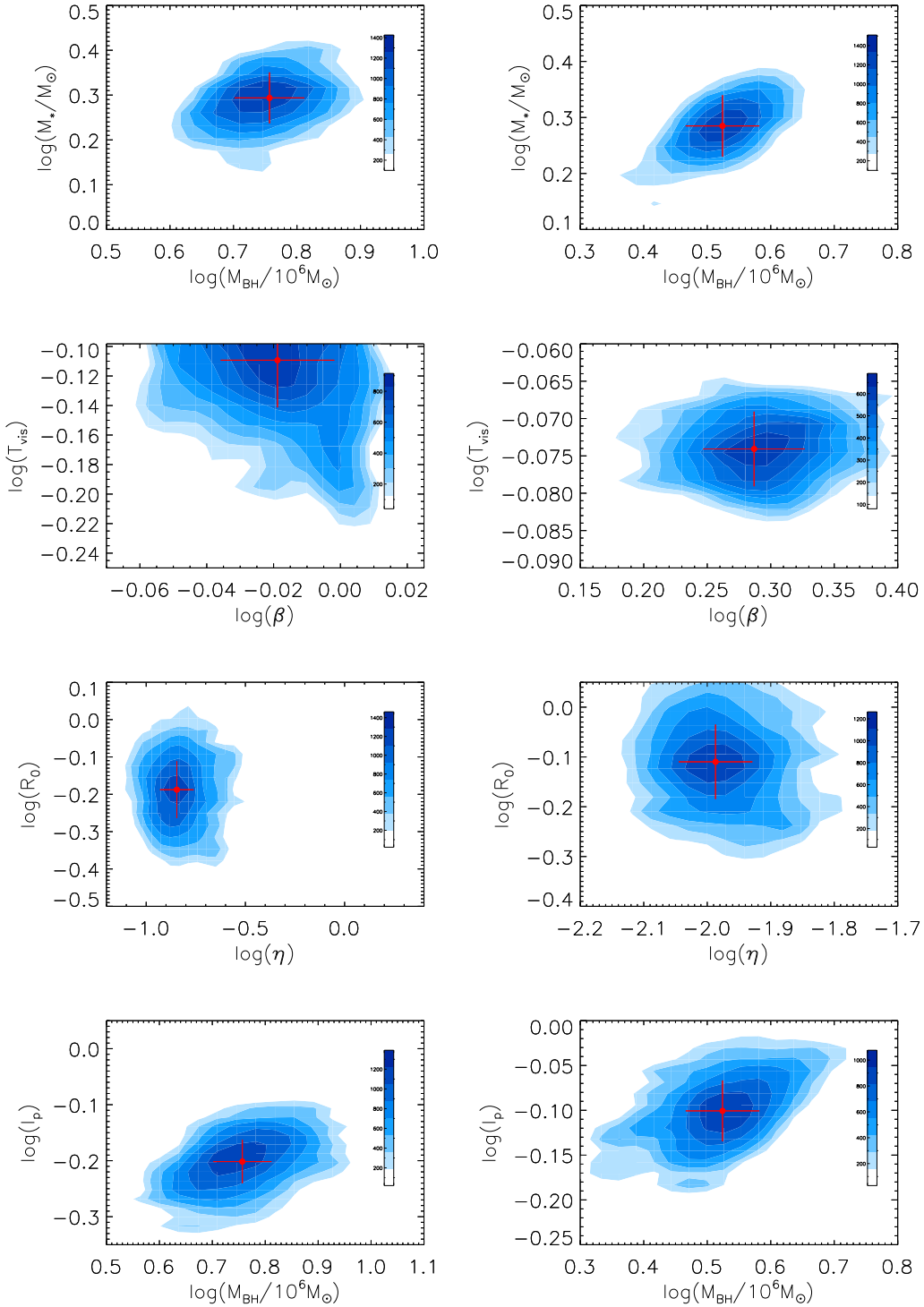


**Figure 3.** MCMC technique determined two dimensional projections of the posterior distributions of the seven model parameters. In each left panel, contour represents the results for the model parameters determined by TDE model with  $\gamma = 4/3$ . In each right panel, contour represents the results for the model parameters determined by TDE model with  $\gamma = 5/3$ . In each panel, solid circle plus error bars in red show the final accepted values and the corresponding uncertainties of the model parameters.

**Table 1.** Parameters of TDE models for SDSS J0159

parameter	prior	p0	value <sup>a</sup>	value <sup>b</sup>
$\log(M_{\text{BH}, 6})$	[-3, 3]	0.	$0.756 \pm 0.055$	$0.524 \pm 0.058$
$\log(M_{\star}/M_{\odot})$	[-2, 1.7]	0.	$0.294 \pm 0.057$	$0.285 \pm 0.055$
$\log(\beta)(4/3)$	[-0.22, 0.6]	0.	$-0.019 \pm 0.017$	...
$\log(\beta)(5/3)$	[-0.3, 0.4]	0.	...	$0.287 \pm 0.042$
$\log(T_{\text{vis}})$	[-3, 0]	-1.	$-0.109 \pm 0.032$	$-0.074 \pm 0.005$
$\log(\eta)$	[-3, -0.4]	-1.	$-0.845 \pm 0.085$	$-1.986 \pm 0.058$
$\log(R_0)$	[-3, 3]	1.	$-0.187 \pm 0.076$	$-0.109 \pm 0.075$
$\log(L_p)$	[-3, 0.6]	0.	$-0.202 \pm 0.039$	$-0.101 \pm 0.034$

Notes: The first column shows the applied model parameters. The second column shows limitations of the prior uniform distribution of each model parameter. The third column with title "p0" lists starting value of each parameter. The fourth column with column title marked with <sup>a</sup> means the values of model parameters for the TDE model with  $\gamma = 4/3$ . The fifth column with column title marked with <sup>b</sup> means the values of model parameters for the TDE model with  $\gamma = 5/3$ .

about 2 of the first data point at MJD-50200=880 to the data points at late times. Therefore, the model with central BH mass larger than  $10^8 M_{\odot}$  are not preferred in SDSS J0159.

Based on the results shown in Fig. 2 and posterior distributions of model parameters shown in Fig. 3, there are two interesting points we can find. First, the observed light curves can be well described by the theoretical TDE model, strongly indicating a TDE around central BH of SDSS J0159 as suggested in Merloni et al. (2015). Second, different model parameters can lead to observed light curves being well described by TDE models, however, the different model parameters in TDE models leading to much different properties on features around peak. In other words, once there were observed high quality light curves with apparent features around peak intensities, the sole TDE model can be determined. Fortunately, due to the similar BH masses in the TDE models with different polytropic indices, it is not necessary to further determine which TDE model, the TDE model with polytropic index  $\gamma = 4/3$  or the model with  $\gamma = 5/3$ , is preferred in SDSS J0159, because only BH mass properties are mainly considered in the manuscript.

Moreover, based on the listed TDE model determined parameters (logarithmic values) in Table 1, the stellar mass of the tidally disrupted main-sequence star is about  $M_{\star} \sim 1.97 M_{\odot}$  ( $M_{\star} \sim 1.93 M_{\odot}$ ) for  $\gamma = 4/3$  ( $\gamma = 5/3$ ), which is out of the transition range between  $0.3 M_{\odot}$  and  $1 M_{\odot}$  for stars as discussed in Mockler et al. (2019). Therefore, we do not consider hybrid fallback functions that smoothly blend between the 4/3 and 5/3 polytopes, as suggested in Mockler et al. (2019). Meanwhile, as the shown best-fitting results to the *ugri*-bands light curves of SDSS J0159 in Fig. 2, applications of the polytropic index  $\gamma = 4/3$  and  $\gamma = 5/3$  individ-

ually can lead to well accepted descriptions to the observed light curves, re-indicating that it is not necessary to describe long-term variabilities of SDSS J0159 with considerations of hybrid fallback functions that smoothly blend between the 4/3 and 5/3 polytopes.

Based on the theoretical TDE model determined BH mass  $M_{\text{BH}} \sim 4.5^{+1.3}_{-1.1} \times 10^6 M_{\odot}$  (the mean value of the two BH masses determined by theoretical TDE models with different polytropic indices), we can check the dependence of BH mass on stellar velocity dispersion in SDSS J0159 in Fig. 4. Comparing with the reported M-sigma relations for both quiescent galaxies in McConnell & Ma (2013); Kormendy & Ho (2013); Savorgnan & Graham (2015) and in AGN in Ho & Kim (2014); Woo et al. (2015), the TDE model determined BH mass is well consistent with the M-sigma relation expected value in SDSS J0159. Moreover, considering the reported BH masses of TDE candidates in Zhou et al. (2021) which we shown as solid cyan circles in Fig. 4, the TDE model determined central BH mass is preferred in SDSS J0159, rather than the virial BH mass about two magnitudes higher than the expected value. Furthermore, Fig. 5 shows the correlation between TDE model determined BH masses  $M_{\text{BH}}$  and TDE model determined energy transfer efficiency  $\eta$  of the TDE candidates in Mockler et al. (2019); Zhou et al. (2021). It is clear that the SDSS J0159 as a radio quiet object is common as the other TDE candidates in the space of  $M_{\text{BH}}$  versus  $\eta$ , besides the TDE candidate *swift* J2058.4+0516 with relativistic jet related to central TDE (Cenko et al. 2012; Zhang 2022a). Therefore, the BH mass about  $10^6 M_{\odot}$  in SDSS J0159 is reasonable enough.

The TDE model determined central BH mass two magnitudes smaller than virial BH mass in SDSS J0159 provide robust evidence to support that the BLRs in SDSS J0159 include strong contributions of accreting debris from central TDE, leading the dynamical properties of disk-like BLRs as discussed in Zhang (2021c). And the results in the manuscript to reconfirm that outliers in the space of virial BH masses versus stellar velocity dispersions could be better candidates of TDEs.

Furthermore, simple discussions are given on variability properties of broad  $H\alpha$ , to support that the Virialization assumption applied to estimate virial BH mass is not appropriate to be applied to estimate central virial BH mass in SDSS J0159. Under the widely accepted virialization assumption for broad line AGN as well discussed in Peterson et al. (2004); Greene & Ho (2005); Vestergaard & Peterson (2006); Kelly & Bechtold (2007); Rafiee & Hall (2011); Shen et al. (2011); Mejia-Restrepo et al. (2022):

$$M_{\text{BH}} \propto V^2 \times R_{\text{BLR}} \propto V^2 \times L^{0.5} \quad (10)$$

where  $V$ ,  $R_{\text{BLR}}$  and  $L$  mean broad line width, distance of BLRs (broad emission line regions) to central BH and broad line



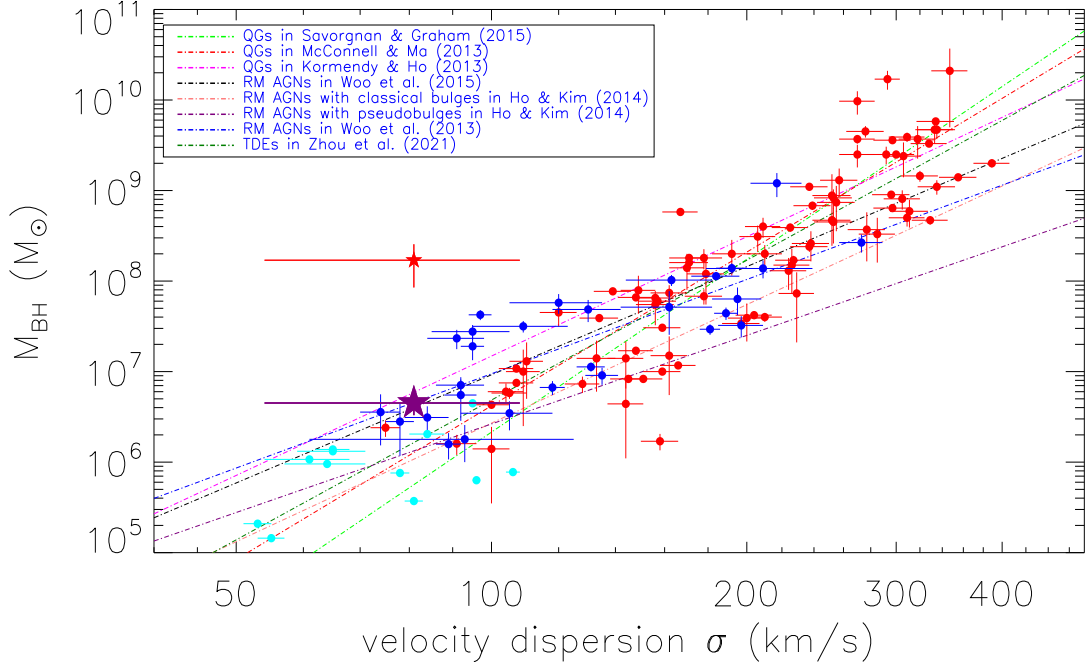


**Figure 4.** On the correlation between stellar velocity dispersions and BH masses. Solid five-point-star in purple shows the BH mass of SDSS J0159 determined by theoretical TDE model and the stellar velocity dispersion measured in the manuscript, solid five-point-star in red shows the virial BH mass of SDSS J0159 as discussed in LaMassa et al. (2015); Merloni et al. (2015); Zhang et al. (2019) and the velocity dispersion measured in Zhang et al. (2019). Dot-dashed lines in different colors listed in the legend in top left corner represent the M-sigma relations reported in the literature through the quiescent galaxies (QGs) and/or the RM (Reverberation Mapped) AGNs with classical/pseudobulges and/or the TDEs. And, solid circles in red, in blue and in cyan show the values for the 89 quiescent galaxies from Savorgnan & Graham (2015), the 29 RM AGNs from Woo et al. (2015) and the 12 TDEs from Zhou et al. (2021), respectively.

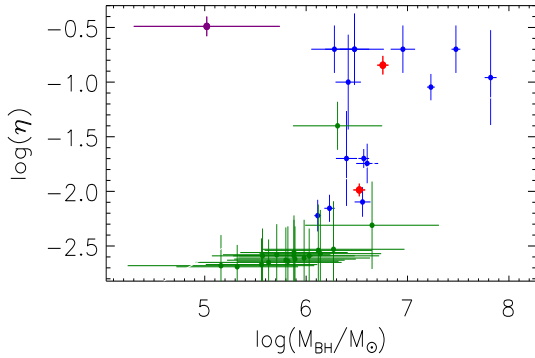


**Figure 5.** On the dependence of energy transfer efficiency  $\eta$  on central BH mass of the reported TDE candidates in Mockler et al. (2019); Zhou et al. (2021). Symbols in blue represent the results collected from Table 2 in Mockler et al. (2019), and symbols in dark green represent the results collected from Table 3 in Zhou et al. (2021). The solid circle plus error bars in purple show the results for the *swift* J2058.4+0516 determined in Zhang (2022a). The two solid circles in red show the determined results by model with  $\gamma = 4/3$  and  $\gamma = 5/3$  in the manuscript, respectively.

luminosity (or continuum luminosity), after accepted the well known empirical R-L relation ( $R_{\text{BLR}} \propto L^{-0.5}$ ) (Kaspi et al. 2005; Bentz et al. 2013). Then for broad H $\alpha$  in multi-epoch spectra of SDSS J0159, we will have

$$V_1^4 \times L_1 = V_2^4 \times L_2 \quad (11)$$

, where suffix 1 and suffix 2 mean parameters from two different epochs. For SDSS J0159 discussed in LaMassa et al. (2015) and Merloni et al. (2015), the widths (full width at half maximum) of broad H $\alpha$  are about  $(3408 \pm 110)$  km/s and  $(6167 \pm 280)$  km/s in 2000 and in 2010, respectively, the luminosities of broad H $\alpha$  are about  $(329 \pm 11) \times 10^{40}$  erg/s and  $(143 \pm 7) \times 10^{40}$  erg/s in 2000 and in 2010, respectively. Thus, the  $V^4 \times L$  in 2000 and 2010 are

$$\left(\frac{V_{2000}}{1000 \text{ km/s}}\right)^4 \times \frac{L_{2000}}{10^{42} \text{ erg/s}} \sim 444_{68}^{77} \quad (12)$$

$$\left(\frac{V_{2010}}{1000 \text{ km/s}}\right)^4 \times \frac{L_{2010}}{10^{42} \text{ erg/s}} \sim 2068_{435}^{523}$$

. There are quite larger  $V^4 \times L$  in 2010 than in 2000. Furthermore, if considering serious obscuration of the broad Balmer lines in 2010 (no broad H $\beta$  detected in 2010), the

luminosity of broad  $H\alpha$  in 2010 should be larger, leading to more larger  $V^4 \times L$  in 2010. The results indicating some none-virial components are actually included in the broad line variabilities, to support our results in the manuscript to some extent.

Before the end of the section, three additional points are noted. First and foremost, as the shown results in Fig. 2, there is a smaller flare around MJD-50200~2700 in SDSS J0159, which can be simply accepted as a re-brightened peak. Among the reported TDEs candidates, ASASSN-15lh reported in [Leloudas et al. \(2016\)](#) is the known TDE candidate with re-brightened peak in its long-term light curves. So far, it is not unclear on the physical origin of re-brightened peaks in TDEs candidates. As discussed in [Leloudas et al. \(2016\)](#), circularization could be efficiently applied to explain re-brightened peak in TDE expected light curves. Meanwhile, as discussed in [Mandel & Levin \(2015\)](#), re-brightened peak could be expected when a binary star is tidally disrupted by a central BH. And as discussed in [Coughlin & Armitage \(2018\)](#), re-brightened peak could be expected when a star is tidally disrupted by a central binary black hole system with extreme mass ratio. Unfortunately, there are not enough information to determine which proposed method is preferred to explain the re-brightened peak around MJD-50200~2700 in SDSS J0159. Further efforts in the near future are necessary to discuss properties of the re-brightened peak in SDSS J0159. And there are no further discussions on the re-brightened peak in SDSS J0159 in the manuscript.

Besides, as the shown and discussed results of the reported optical TDEs candidates in [Mockler et al. \(2019\)](#); [Gezari \(2021\)](#); [van Velzen et al. \(2021\)](#), time durations about hundreds of days in rest frame can be found at 10% of the peak of the TDE expected light curves, quite smaller than the corresponding time duration of about 1900days at 10% of the peak of the light curves of the SDSS J0159 in the rest frame (with redshift  $z=0.312$  accepted). Actually, the longer time duration in SDSS J0159 can be naturally explained by the scaled relation in equation (6) with different BH mass and stellar mass. As an example, among the reported optical TDEs candidates shown in [Mockler et al. \(2019\)](#), the PTF09ge has time duration about  $T_P \sim 160days$  at 10% (2.5magnitudes weaker than the peak magnitude) of the peak of its light curves in the rest frame. The PTF09ge is collected, mainly due to more clearer and smoother optical light curves with larger variability amplitudes shown in Fig. 1 in [Mockler et al. \(2019\)](#). To collect one another TDE candidate can lead to similar results. Considering PTF09ge with MOSFIT determined BH mass about  $M_{BH,P} \sim 3.6 \times 10^6 M_\odot$  and stellar mass about  $M_{\star,P} \sim 0.1 M_\odot$  (corresponding stellar radius about  $R_{\star,P} \sim 0.12 R_\odot$ ) and  $\beta_P \sim 1.1$  and  $\gamma_P = 5/3$  listed in [Mockler et al. \(2019\)](#), the expected time duration  $T_S$  of the

TDE expected light curve in SDSS J0159 can be estimated as

$$T_S \sim T_P \left( \frac{M_{BH,S}}{M_{BH,P}} \right)^{0.5} \left( \frac{M_{\star,S}}{M_{\star,P}} \right)^{-1} \left( \frac{R_{\star,S}}{R_{\star,P}} \right)^{1.5} S_\beta \quad (13)$$

with  $S_\beta$  as the parameter considering effects of different  $\beta$  applied in PTF09ge ( $\beta_P \sim 1.1$ ) and in SDSS J0159 ( $\beta_S \sim 1.94$ ). Then, based on the determined parameters listed in Table 1 for SDSS J0159 with  $\gamma_S = 5/3$ , the central BH mass and stellar parameters are about  $M_{BH,S} \sim 3.4 \times 10^6 M_\odot$  and  $M_{\star,S} \sim 1.93 M_\odot$  (corresponding stellar radius about  $R_{\star,S} \sim 1.51 R_\odot$ ). Meanwhile, based on light curves of the created standard templates of time-dependent viscous-delayed accretion rates with  $\gamma = 5/3$  and  $M_{BH} = 10^6 M_\odot$  and  $M_\star = 1 M_\odot$ , time duration at 10% of the peak of the light curve of the viscous-delayed accretion rate with  $\beta = 1.94$  and  $\log(T_{vis} \sim -0.074)$  (the values for the SDSS J0159) is about 1280days, about 4.7 times longer than the corresponding time duration about 280days with  $\beta = 1.1$  and  $\log(T_{vis} \sim -1.4)$  (the values for the PTF09ge), leading to  $S_\beta \sim 4.6$ . Then, based on the parameters for PTF09ge and for SDSS J0159, we can have

$$T_S \sim 160 \left( \frac{3.4}{3.6} \right)^{0.5} \left( \frac{0.1}{1.93} \right) \left( \frac{1.51}{0.12} \right)^{1.5} 4.6 \sim 1700days \quad (14)$$

very similar as the time duration 1900days at 10% of the peak of the TDE expected flare in the SDSS J0159. The results strongly indicate that the longer time durations of the TDE expected flare in SDSS J0159 are reasonable.

Last but not the least, as discussed in [Merloni et al. \(2015\)](#), there are expected AGN activities through applications of narrow emission line flux ratios (see their Fig. 3). Therefore, the central TDE in SDSS J0159 is a central TDE in AGN host galaxy, quiet different from the vast majority of the reported optical TDEs candidates in quiescent galaxies. Actually, there are so-far only hands of TDEs candidates reported in AGN host galaxies. [Blanchard et al. \(2017\)](#) have reported a TDE candidate in a narrow line Seyfert 1 galaxy of which light curves can be roughly described by theoretical TDE model. [Yan & Xie \(2018\)](#) have shown the TDE expected variability pattern in the low-luminosity AGN NGC 7213. [Liu et al. \(2020\)](#) have reported a TDE candidate in AGN SDSS J0227. [Frederick et al. \(2021\)](#) have reported TDEs candidates in narrow line Seyfert 1 galaxies. More recently, [Zhang et al. \(2022\)](#) have shown the TDE expected variability patterns in a narrow line Seyfert 1 galaxy. Meanwhile, [Chan et al. \(2019, 2020\)](#) have modeled TDEs variabilities in AGN with a pre-existing accretion disc, and shown that about 20days-long plateau could be expected around central BH with masses around  $10^{6-7} M_\odot$ . Therefore, considering variability properties of the detected optical TDEs candidates in AGN host galaxy reported in the literature, TDE expected variability patterns can also be expected in SDSS J0159. Even

considering the 20days-long plateau feature by simulating results in Chan et al. (2020), the plateau has few effects on the long-term variabilities of SDSS J0159, because the time duration about 1900days of the light-curves of SDSS J0159 is quite larger than 20days. In one word, the expected central TDE in SDSS J0159 is in AGN host galaxy, but TDE described variability patterns can be well expected in SDSS J0159.

## 5. WHETHER THE LONG-TERM VARIABILITIES ARE RELATED TO CENTRAL AGN ACTIVITIES IN SDSS J0159?

The results and discussions above are mainly based on the fundamental point that the long-term variabilities are related to a central TDE in SDSS J0159. Therefore, it is necessary and interesting to check probability of AGN activities applied to well describe the long-term variabilities in SDSS J0159. Here, in order to compare variability properties between SDSS J0159 and the other normal quasars in the literature MacLeod et al. (2010), rather than the luminosity light curve but the photometric light curve is mainly discussed in the section.

The known Continuous AutoRegressive (CAR) process and/or the improved Damped Random Walk (DRW) process can be applied to describe intrinsic AGN activities, as well discussed in Kelly, Bechtold & Siemiginowska (2009); Kozłowski et al. (2010); MacLeod et al. (2010); Zu et al. (2013, 2016); Zhang & Feng (2017); Moreno et al. (2019); Sheng, Ross & Nicholl (2022). Here, based on the DRW process, the collected photometric  $g$ -band light curve from Stripe82 database (Bramich et al. 2008; Thanjavur et al. 2021) can be described by the public code JAVELIN (Just Another Vehicle for Estimating Lags In Nuclei) (Kozłowski et al. 2010; Zu et al. 2013), with two process parameters of intrinsic characteristic variability amplitude and timescale of  $\sigma$  and  $\tau$ . The best descriptions are shown in left panel of Fig. 6. And corresponding MCMC technique determined two dimensional posterior distributions of  $\sigma$  and  $\tau$  are shown in right panel of Fig. 6, with the determined  $\log(\tau/\text{days}) \sim 2.92 \pm 0.21$  and  $\log(\sigma/(\text{mag}/\text{days}^{0.5})) \sim -0.55 \pm 0.10$ , leading  $SF_\infty/\text{mag} \sim \sigma/(\text{mag}/\text{days}^{0.5}) \times \sqrt{\tau/\text{days}}$  to be about  $\log(SF_\infty/\text{mag}) \sim 0.85$  in SDSS J0159. Actually, to collect the photometric  $uri$ -band light curves can lead to similar results. Meanwhile, as discussed in MacLeod et al. (2010) for SDSS normal quasars in Stripe82 database, normal SDSS quasars have mean values of  $\log(\tau/\text{days}) \sim 2.4$  and  $\log(SF_\infty/\text{mag}) \sim -0.7$ . Therefore, in the space  $\log(\tau)$  versus  $\log(SF_\infty)$ , SDSS J0159 is an outlier among the quasars, due to its  $\log(SF_\infty/\text{mag})$  about 1.5magnitudes larger than the normal quasars. In other words, although the SDSS J0159 has its light curves with longer time durations, SDSS J0159 has

unique variability properties, quite different from the normal SDSS quasars.

Moreover, besides the discussions in the section to show unique variability properties in SDSS J0159, two additional points can be found. First, the first data point at MJD-50200=880 is apparently 0.3magnitudes brighter than the data points with MJD-50200 later than 4000, which can be applied as one another evidence to support that the first data point at MJD-50200=880 in Fig. 2 is not one data point similar as the other data points at late times, but one data point related to the central TDE, under the assumed TDE to explain variabilities of SDSS J0159, similar as discussed results in Section 4. Second, although there are unique variability properties in SDSS J0159 quite different from normal quasars, contributions of central AGN activities to the light curves cannot be totally ruled out, such as the shown weak AGN activities in eBOSS spectrum of SDSS J0159. Therefore, it is necessary to discuss effects of central AGN activities on our final results. Besides the fitting procedure discussed in Section 3, five additional model parameters are added to described AGN contributions to the light curves, i.e., the equation (8) in Section 3 is re-written to

$$L_{u, g, r, i, z}(t) = \int_{\lambda_{u, g, r, i, z}} f_\lambda(t) d\lambda \times 4\pi \times Dis^2 + L_{0, u, g, r, i, z} \quad (15)$$

with  $L_{0, u, g, r, i, z} > 0$  as the AGN contributions. Then, the theoretical TDE model with 12 model parameters are applied to re-describe the  $ugriz$ -band luminosity light curves shown in Fig. 2 through the Levenberg-Marquardt least-squares minimization technique, leading to the parameters  $L_{0, u, g, r, i, z} \sim 0$  and similar BH masses as discussed in Section 4, because the data points at late times have luminosities around zero as shown in Table 2 in Merloni et al. (2015). If parameters of  $L_{0, u, g, r, i, z}$  are not constant values but time-dependent, corresponding fitting results to  $ugr$ -band luminosity light curves could lead to stronger luminosities at data points earlier than MJD-50200=880, quite brighter than the data points from POSSII shown in Fig. 1 in Merloni et al. (2015). Therefore, even there are weak AGN activities, they have few effects on our final results through applications of theoretical TDE model in the manuscript.

## 6. MAIN SUMMARY AND CONCLUSIONS

Finally, we give our main summary and conclusions as follows.

- Host galaxy spectroscopic features are measured by the simple SSP method applied with 350 stellar templates, to confirm the low total stellar mass of SDSS J0159, through the whole spectroscopic absorption features within rest wavelength range from 3650Å to 7700Å.

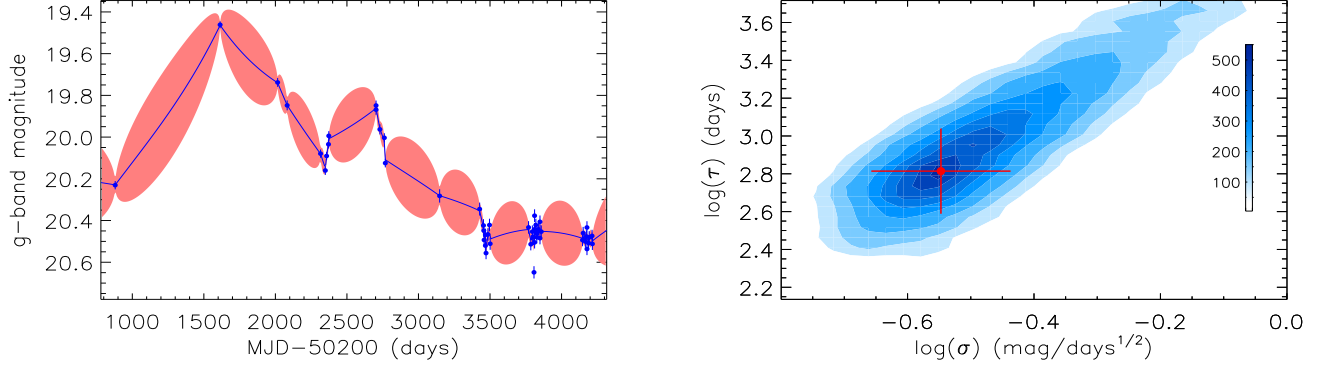


**Figure 6.** Left panel shows the JAVELIN code determined best descriptions to the long-term photometric  $g$ -band (solid circles plus error bars in blue) light curve of SDSS J0159. Solid blue line and area filled in pink show the best descriptions and corresponding  $1\sigma$  confidence bands to the  $g$ -band luminosity light curve. Right panel shows the MCMC technique determined two-dimensional posterior distributions in contour of  $\ln(\tau/\text{days})$  and  $\ln(\sigma/(\text{mag}/\text{days}^{0.5}))$ , with solid circle plus error bars in red showing the accepted values and  $1\sigma$  uncertainties of  $\ln(\tau)$  and  $\ln(\sigma)$ .

- Theoretical TDE model can be well applied to describe the  $ugriz$ -band variabilities of SDSS J0159, leading the central BH mass to be about  $M_{BH} \sim 4.5_{-1.1}^{+1.3} \times 10^6 M_{\odot}$ , two magnitudes smaller than the virial BH mass in SDSS J0159.
- Through CAR/DRW process applied to describe long-term light curves of SDSS J0159, comparing variability properties between SDSS J0159 and the normal SDSS quasars in Stripe82 database, SDSS J0159 is an outlier in the space of the process parameter of intrinsic variability timescale  $\tau$  versus intrinsic variability amplitude  $\sigma$ , indicating SDSS J0159 has unique variability properties, quite different from the normal quasars.
- Theoretical TDE model with the model parameter of central BH mass limited to be higher than  $10^8 M_{\odot}$  cannot lead to reasonable descriptions to the SDSS  $ugri$ -band variabilities of SDSS J0159, indicating central BH mass higher than  $10^8 M_{\odot}$  is not preferred in SDSS J0159.
- The TDE model determine central BH mass is well consistent with the  $M$ - $\sigma$  relation expected value through the measured stellar velocity dispersion in SDSS J0159.
- The outliers in the space of virial BH masses versus stellar velocity dispersions could be better candidates of TDEs.

#### ACKNOWLEDGEMENTS

Zhang gratefully acknowledge the anonymous referee for giving us constructive comments and suggestions to greatly improve our paper. Zhang gratefully thanks the research funding support from GuangXi University and the grant support from NSFC-12173020. This manuscript has made use of the data from the SDSS projects. The SDSS-III web site is <http://www.sdss3.org/>. SDSS-III is managed by the Astrophysical Research Consortium for the Participating Institutions of the SDSS-III Collaboration. The paper has made use of the public code of TDEFIT (<https://github.com/guillochon/tdefit>) and MOSFIT (<https://github.com/guillochon/mosfit>), and use of the MPFIT package (<http://cow.physics.wisc.edu/~craigm/idl/idl.html>) written by Craig B. Markwardt, and use of the python emcee package (<https://pypi.org/project/emcee/>). The paper has made use of the template spectra for a set of SSP models from the MILES <https://miles.iac.es>.

#### REFERENCES

- Abdurro'uf; Katherine, A.; Conny, A.; et al., 2022, ApJS, 259, 35  
 Ahumada, R.; Prieto, C. A.; Almeida, A.; et al., 2020, ApJS, 249, 3  
 Bennert, V. N., et al., 2015, ApJ, 809, 20  
 Bentz M. C., Denney K. D., Grier C. J., et al., 2013, ApJ, 767, 149  
 Blanchard, P. K.; Nicholl, M.; Berger, E.; et al., 2017, ApJ, 843, 106  
 Bogdanovic T., Eracleous M., Mahadevan S., Sigurdsson S., Laguna P., 2004, ApJ, 610, 707  
 Bonnerot C., Price D. J., Lodato G., Rossi E. M., 2017, MNRAS, 649, 4879  
 Bramich, D. M.; Vidrih, S.; Wyrzykowski, L.; et al., 2008, MNRAS, 386, 887

- Bruzual, A. G.; Charlot, S., 1993, *ApJ*, 405, 538
- Bruzual, G., & Charlot, S. 2003, *MNRAS*, 344, 1000
- Cappellari, M.; Emsellem, E., 2004, *PASP*, 116, 138
- Cappellari, M., 2017, *MNRAS*, 466, 798
- Cenko S. B.; Krimm, H. A.; Horesh, A.; et al., 2012, *ApJ*, 753, 77
- Chan, C.-H.; Piran, T.; Krolik, J. H.; Saban, D., 2019, *ApJ*, 881, 113
- Chan, C. H.; Piran, T.; Krolik, J. H., 2020, *ApJ*, 903, 17
- Charlton, P. J. L.; Ruan, J. J.; Haggard, D.; Anderson, S. F.; Eracleous, M.; MacLeod, C. L.; Runnoe, J. C., 2019, *ApJ*, 876, 75
- Cid Fernandes, R.; Mateus, A.; Sodre, L.; Stasinska, G.; Gomes, J. M., 2005, *MNRAS*, 358, 363
- Cid Fernandes, R.; Perez, E.; Garcia Benito, R.; et al., 2013, *A&A*, 557, 86
- Coughlin, W. R.; Armitage, P. J., 2018, *MNRAS*, 474, 3857
- Coughlin, E. R.; Nixon, C. J., 2019, *ApJL*, 883, 17
- Curd B. & Narayan R., 2019, *MNRAS*, 483, 565
- Darbha S., Coughlin E. R., Kasen D., Quataert E., 2018, *MNRAS*, 477, 4009
- Drake, A. J.; Djorgovski, S. G.; Mahabal, A., et al., 2009, *ApJ*, 696, 870
- Evans C. R., & Kochanek C. S., 1989, *ApJL*, 346, 13
- Falcon-Barroso, J.; Sanchez-Blazquez, P.; Vazdekis, A.; et al., 2001, *A&A*, 535, 95
- Foreman-Mackey D. Hogg D. W., Lang D., Goodman J., 2013, *PASP*, 125, 306
- Frederick, S.; Gezari, S.; Graham, M. J.; et al., 2021, *ApJ*, 920, 56
- Ferrarese, F.; Merritt, D., 2000, *ApJL*, 539, 9
- Gebhardt, K.; Bender, R.; Bower, G.; et al., 2000, *ApJL*, 539, 13
- Gezari S.; Chornock, R.; Rest, A.; et al., 2012, *Nature*, 485, 217
- Gezari S., 2021, *ARA&A*, 59, 21
- Golightly, E. C. A.; Coughlin, E. R.; Nixon, C. J., 2019, *ApJ*, 872, 163
- Goodwin, A. J.; van Velzen, S.; Miller-Jones, J. C. A.; et al., 2022, 511, 5328
- Graur, O.; French, K. D.; Zahid, H. J.; et al., 2018, *ApJ*, 853, 39
- Greene, J. E. & Ho, L. C., 2005, *ApJ*, 630, 122
- Guillochon J. & Ramirez-Ruiz E., 2013, *ApJ*, 767, 25
- Guillochon J., Manukian H. & Ramirez-Ruiz E., 2014, *ApJ*, 783, 23
- Guillochon J. & Ramirez-Ruiz E., 2015, *ApJ*, 809, 166
- Guillochon, J.; Nicholl, M.; Villar, V. A.; Mockler, B.; Narayan, G.; Mandel, K. S.; Berger, E.; Williams, P. K., 2018, *ApJS*, 236, 6
- Haring, N.; Rix, H. W., 2004, *ApJL*, 604, 89
- Holoien T. W. S.; Prieto, J. L.; Bersier, D.; et al., 2014, *MNRAS*, 445, 323
- Holoien T. W. S.; Kochanek, C. S.; Prieto, J. L.; et al., 2016, *MNRAS*, 455, 2918
- Holoien, T. W. S.; Auchettl, K.; Tucker, M. A.; et al., 2020, *ApJ*, 898, 161
- Kauffmann, G.; Heckman, T. M.; White, S. D. M.; Charlot, S.; Tremonti, C.; et al., 2003b, *MNRAS*, 341, 54
- Ho, L. C. & Kim, M.-J., 2014, *ApJ*, 789, 17
- Jiang, N.; Wang, T. G.; Yan, L.; et al., 2017, *ApJ*, 850, 63
- Jiang, N.; Wang, T. G.; Hu, X. Y.; Sun, L. M.; Dou, L. M.; Xiao, L., 2021, *ApJ*, 911, 31
- Kaspi, S.; Maoz, D.; Netzer, H.; Peterson, B. M.; Vestergaard, M.; Jannuzi, B. T., 2005, *ApJ*, 629, 61
- Kelly, B. C., & Bechtold, J., 2007, *ApJS*, 168, 1
- Kelly, B. C.; Bechtold, J.; Siemiginowska, A., 2009, *ApJ*, 698, 895
- Komossa S.; Halpern, J.; Schartel, N.; Hasinger, G.; Santos-Lleo, M.; Predehl, P., 2004, *ApJL*, 603, 17
- Kormendy, J. & Ho, L. C., 2013, *ARA&A*, 51, 511
- Kozłowski, S.; Kochanek, C. S.; Udalski, A., et al., 2010, *ApJ*, 708, 927
- Knowles, A. T.; Sansom, A. E.; Allende Prieto, C.; Vazdekis, A., 2021, *MNRAS*, 504, 2286
- LaMassa S. M.; Cales, S.; Moran, E. C.; et al., 2015, *ApJ*, 800, 144
- Leloudas, G.; Fraser, M.; Stone, N. C.; et al., 2016, *Natur Astronomy*, 1, 2
- Lin D., Guillochon J., Komossa S., et al., 2017, *Natur Astronomy*, 1, 33
- Liu, Z.; Li, D.; Liu, H.; et al., 2020, *ApJ*, 894, 93
- Lodato G., King A. R. & Pringle J. E., 2009, *MNRAS*, 392, 332
- Lodato G., Franchini A., Bonnerot C., Rossi E. M., 2015, *JHEAp*, 7, 158
- Lopez Fernandez, R.; Cid Fernandes, R.; Gonzalez Delgado, R. M.; et al., 2016, *MNRAS*, 458, 184
- Lu, W. B.; Kumar, P.; Evans, N. J., 2016, *MNRAS*, 458, 575
- MacLeod, C. L., Ivezić, Z., Kochanek, C. S., et al., 2010, *ApJ*, 721, 1014
- Mejia-Restrepo, J. E.; Trakhtenbrot, B.; Koss, M. J., et al., 2022, *ApJS*, 261, 5
- McConnell, N. J. & Ma, C. P., 2013, *ApJ*, 764, 184
- MacLeod M., Guillochon J. & Ramirez-Ruiz E., 2012, *ApJ*, 757, 134
- Magorrian J. & Tremaine S., 1999, *MNRAS*, 309, 447
- Mandel, I.; Levin, Y., 2015, *ApJL*, 805, 4
- Mattila S., Perez-Torres M., Efstathiou A., et al., 2018, *Sci*, 361, 482
- Merloni A., et al., 2015, *MNRAS*, 452, 69
- Mockler B.; Guillochon J.; Ramirez-Ruiz E., 2019, *ApJ*, 872, 151
- Moreno, J.; Vogeley, M. S.; Richards, G. T.; Yu, W., 2019, *PASP*, 131, 3001
- Neustadt, J. M. M.; Holoien, T. W. S.; Kochanek, C. S.; et al., 2020, *MNRAS*, 494, 2538
- Peterson B. M., Ferrarese L., Gilbert K. M., et al. 2004, *ApJ*, 613, 682
- Rafiee A. & Hall P. B., 2011, *ApJS*, 194, 42
- Rees M. J., 1988, *Nature*, 333, 523

- Reines, A. E.; Volonteri, M., 2015, *ApJ*, 813, 82
- Ryu, T.; Krolik, J.; Piran, T., 2020, *ApJ*, 904, 73
- Sani, E., Marconi, A., Hunt, L. K., Risaliti, G. 2011, *MNRAS*, 413, 1479
- Sazonov, S.; Gilfanov, M.; Medvedev, P.; et al., 2021, *MNRAS*, 508, 3820
- Savorgnan, G. A. D. & Graham, A. W., 2015, *MNRAS*, 446, 2330
- Shen, Y.; Richards, G. T.; Strauss, M. A.; et al., 2011, *ApJS*, 194, 45
- Sheng, X.; Ross, N.; Nicholl, M., 2022, *MNRAS*, 512, 5580
- Stone N. C., Kesden M., Chang R. M., van Velzen S., *General Relativity and Gravitation*, 2018, arXiv:1801.10180
- Tadhunter C., Spence R., Rose M., Mullaney J., Crowther P., 2017, *Natur Astronomy*, 1, 61
- Thanjavur, K.; Ivezic, Z.; Allam, S. S.; Tucker, D. L.; Smith, J. A.; Gwyn, S., 2021, *MNRAS*, 505, 5941
- Tout, C. A.; Pols, O.; Eggleton, P.; Han, Z., 1996, *MNRAS*, 281, 257
- van Velzen, S.; Gezari, S.; Hammerstein, E.; et al., 2021, *ApJ*, 908, 4
- Vestergaard, M. & Peterson, B. M., 2006, *ApJ*, 641, 689
- Wang T.-G.; Yan, L.; Dou, L.; Jiang, N.; Sheng, Z.; Yang, C., *MNRAS*, 2018, 477, 2943
- Werle, A.; Cid Fernandes, R.; Vale Asari, N.; Bruzual, G.; Charlot, S.; Gonzalez Delgado, R.; Herpich, F. R., 2019, *MNRAS*, 483, 2382
- Wevers T., van Velzen S., Jonker P. G., et al., *MNRAS*, 2017, 471, 1694
- Wong, T. H. T.; Pfister, H.; Dai, L., 2022, *ApJL*, 927, 19
- Woo, J.-H.; Schulze, A.; Park, D.; Kang, W.; Kim, S.; Riechers, D. A., 2013, *ApJ*, 772, 49
- Woo, J.-H.; Yoon, Y.; Park, S.; Park, D.; Kim, S. C., 2015, *ApJ*, 801, 38
- Yan, Z.; Xie, F., 2018, *ApJ*, 475, 1190
- Yang, Q.; Wu, X.; Fan, X.; et al., 2018, *ApJ*, 862, 109
- Zhang, W. J.; Shu, X. W.; Sheng, Z. F., et al., 2022, *A&A*, 660, 119
- Zhang, X. G., 2014, *MNRAS*, 438, 557
- Zhang, X. G.; Feng L. L., 2017, *MNRAS*, 464, 2203
- Zhang, X. G.; Bao, M.; Yuan, Q. R., 2019, *MNRAS Letter*, 490, 81
- Zhang, X. G., 2021a, *ApJ*, 909, 16, ArXiv:2101.02465
- Zhang, X. G., 2021b, *ApJ*, 919, 13, Arxiv:2107.09214
- Zhang, X. G., 2021c, *MNRAS Letter*, 500, 57, Arxiv:2011.06213
- Zhang, X. G., 2022a, *ApJ*, 928, 182, Arxiv:2202.11265
- Zhang, X. G., 2022b, *MNRAS Letter*, 516, 66, Arxiv:2208.05253
- Zhang, X. G., 2022c, *MNRAS Letter*, 517, 71, Arxiv:2209.09037
- Zhou, Z. Q.; Liu, F. K.; Komossa, S., et al., 2021, *ApJ*, 907, 77
- Zu, Y.; Kochanek, C. S.; Kozłowski, S.; Udalski, A., 2013, *ApJ*, 765, 106
- Zu, Y.; Kochanek, C. S.; Kozłowski, S.; Peterson, B. M., 2016, *ApJ*, 819, 122